Frontiers of Information Technology & Electronic Engineering
www.jzus.zju.edu.cn; engineering.cae.cn; www.springerlink.com
ISSN 2095-9184 (print); ISSN 2095-9230 (online)
E-mail: jzus@zju.edu.cn

Joint target tracking using an autonomous underwater vehicle and underwater sensor networks for underwater applications*

Zhaohong LV[1], Zhenkai ZHANG‡[1], Boon-Chong SEET[2], Yi YANG[3]

[1]*Ocean College, Jiangsu University of Science and Technology, Zhenjiang 212003, China*

[2]*Electrical and Electronic Engineering Department, Auckland University of Technology, Auckland 1010, New Zealand*

[3]*Wuhan Maritime Communication Research Institute, Wuhan 430223, China*

E-mail: 1921301805@qq.com; zhangzhenkai@just.edu.cn; boon-chong.seet@aut.ac.nz; 88563379@qq.com

Received Sept. 22, 2024; Revision accepted Nov. 18, 2024; Crosschecked July 17, 2025

Abstract: Because underwater sensor networks (USNs) have limited energy resources due to environmental constraints, it is essential to improve energy utilization. For this purpose, an autonomous underwater vehicle (AUV) with greater onboard computation power is used to process measurement data, and the mobility of the AUV is leveraged to optimize the USN topology, enhancing tracking accuracy. First, to address the transmission delay of underwater acoustic signals, a time-delay compensated centralized extended Kalman filter (TD-CEKF) algorithm is proposed. Next, the mathematical relationship between AUV position and USN topology is established, based on which the optimization target is constructed. Subsequently, a penalty function is introduced to remove the constraints from the objective function, and the optimal AUV position is searched using the gradient descent method to optimize the USN topology. The simulation results demonstrate that the proposed algorithm can effectively overcome the influence of transmission delay on target tracking and achieve improved tracking performance.

Key words: Underwater sensor networks (USNs); Target tracking; Time delay estimation; Autonomous underwater vehicle (AUV)
https://doi.org/10.1631/FITEE.2400869 **CLC number:** TN92

1 Introduction

With the increasing emphasis on marine resources and security, the Internet of Underwater Things (IoUT) has gradually started to take shape (Jahanbakht et al., 2021). As an early practical form of IoUT, underwater sensor networks (USNs) have been widely used in underwater resource exploration, marine environmental monitoring, and marine military applications (Alostad, 2020; Mohsan et al., 2022). Among them, target tracking technology based on USNs has become a research hotspot due to its stealth, low cost, and flexibility, and it has been applied in scenarios such as diver navigation, underwater search and rescue, and hostile target monitoring (Tang et al., 2024). Target tracking technology based on USNs faces two main challenges—the complex underwater acoustic environment, characterized by narrow bandwidth and significant transmission delays, which makes tracking difficult, and energy constraints on USN nodes, which cannot have their batteries replaced, resulting in a limited lifetime. The problem of limited bandwidth resources in underwater acoustic channel communication can be addressed by improving the communication bandwidth utilization rate. Zhang SL et al. (2017) quantized the sensor communication data to reduce the communication bandwidth occupation and improved the quantization error by selecting quantization bounds. Luo et al. (2019) further improved underwater target

‡ Corresponding author

* Project supported by the National Natural Science Foundation of China (No. 61871203) and the Postgraduate Research & Practice Innovation Program of Jiangsu Province (Nos. KYCX24_4174 and SJCX24_2606)

ORCID: Zhaohong LV, https://orcid.org/0009-0001-1136-9888; Zhenkai ZHANG, https://orcid.org/0000-0003-2439-0923; Boon-Chong SEET, https://orcid.org/0000-0002-9511-7521

tracking performance by selecting different quantization bits for different sensor nodes. Zhang Q et al. (2015) derived the Cramér–Rao lower bound under quantized measurements and used it as an optimization objective to select the best fusion node to improve the tracking performance. To address the issue of transmission delays in underwater acoustic signals, Su et al. (2020) considered the impact of transmission delay of ranging echoes and proposed an unscented Kalman filter (UKF) fusion method based on delay estimation. On this basis, Zhang ZK et al. (2023) improved the calculation of transmission delay and proposed an improved asynchronous fusion method for particle filters.

Many studies have focused on improvements in the energy utilization of USNs. Li et al. (2025) used the topological structure and energy consumption of nodes as indicators to select neighboring nodes for tracking, thereby reducing energy consumption while meeting tracking accuracy requirements. Zhang D et al. (2019) studied the relationship between node transmission energy consumption and the Fisher information matrix (FIM), on the basis of which the energy of sensor nodes in a period of time is reasonably allocated. Tian and Zhang (2022) considered the errors caused by the positional uncertainty of USNs. Using the FIM, mutual information, and the number of nodes as objectives, they employed the non-dominated sorting genetic algorithm II (NSGA-II) and the technique for order preference by similarity to ideal solution (TOPSIS) to select specific nodes for tracking, thereby reducing the energy consumption of the sensor network. Zheng et al. (2023) proposed a reinforcement learning sensor node selection scheme to achieve a balance between tracking accuracy and energy consumption through a trained dueling double deep Q-network (D3QN). Zhang D et al. (2018) fully mined the information of measured values, calculated the mutual information of sensor nodes, and proposed a data fusion method based on mutual information weighting.

Most of the above studies focus on traditional fixed USNs, where the nodes are immobile and the coverage area and battery capacity are limited. However, autonomous underwater vehicles (AUVs) have relatively mature applications in scientific research, civilian use, and military fields (Xu and Guo, 2022; Xu et al., 2022; Zhang JX et al., 2022; Wang et al., 2024). Compared to fixed USN nodes, AUVs have the capability of free movement and possess greater computing power. More importantly, AUVs can surface for recovery and recharge after completing their tasks. Therefore, by introducing AUVs into the tracking process, the energy consumption of USN nodes can be reduced, and the tracking performance can be improved. At present, research on AUV underwater target tracking applications is focused on single AUV or multi-AUV collaboration (Chen et al., 2022a, 2022b), and there is little research on joint tracking by AUV and USN nodes (Song et al., 2023). Although Tian and Zhang (2021) used the AUV's mobility and computing power to act as a fusion center in the proposed tracking method, their research did not consider the influence of the AUV's own position change on the USN topology.

Although the aforementioned literature on delay estimation fusion has effectively improved underwater target tracking through particle simulation of acoustic transmission delays, tracking methods based on particle Monte Carlo simulation and unscented transformation require extensive computation. This places high demands on the computational capabilities of USNs, making it difficult to meet the requirements of practical engineering applications. The aforementioned research on improving the energy efficiency of USNs has greatly enhanced energy utilization during target tracking. However, these studies have focused primarily on traditional fixed USNs, with relatively few in-depth investigations into the collaboration between AUVs and USNs. Motivated by this, a target tracking method involving the collaboration between AUVs and USNs is proposed in this paper. On the basis of using an AUV's computing power to make it a fusion center, the AUV is used as a tracking node to reduce the number of USN nodes participating in tracking and improve the lifetime of USNs. Then, the mobility of the AUV is used to form a better topology with the USN nodes involved in tracking to improve the tracking performance.

The main contributions of this paper are as follows:

1. A time-delay compensated centralized extended Kalman filter (TD-CEKF) method for cooperative tracking by AUV and USN nodes is proposed. This method not only considers the influence of the underwater acoustic signal transmission delay but also avoids the simulation of many particles.

2. The mathematical relationship between AUV position coordinates and the FIM is derived, and the optimization problem is constructed on this basis.

3. An AUV position search algorithm based on the gradient descent method is proposed. First, the problem is unconstrained by applying a penalty function, and then the AUV position with the best topology is searched using gradient descent.

2 System model

In this section, the motion model of the target and the measurement model of the sensors are established, and the underwater acoustic signal transmission model and the TD-CEKF algorithm are introduced.

2.1 USN and underwater target motion model

We assume that all sensor clocks and measurement times are synchronized and that the measurement information includes timestamps. The target moves in the underwater three-dimensional (3D) space, and the state of the target at time k is

$$\boldsymbol{X}_k=[x_k, v_{x,k}, y_k, v_{y,k}, z_k, v_{z,k}]^{\mathrm{T}}, \tag{1}$$

where (x_k, y_k, z_k) is the 3D coordinates of the target at time k and $(v_{x,k}, v_{y,k}, v_{z,k})$ is the velocity vector of the target.

The motion equation of the target at time k can be expressed as

$$\boldsymbol{X}_{k+1}=\boldsymbol{F}_k\boldsymbol{X}_k+\boldsymbol{G}_k\boldsymbol{w}_k, \tag{2}$$

where $\boldsymbol{F}_k$ is the state transition matrix of the target's motion. In USN target tracking, common motion models include constant velocity (CV) and constant turn (CT). $\boldsymbol{G}_k$ represents the process noise matrix and $\boldsymbol{w}_k$ is the zero-mean Gaussian white noise. The sampling interval is T, and the state transition matrix $\boldsymbol{F}_k$ of the two motion models can be expressed as

$$\boldsymbol{F}_k^{\mathrm{CV}}=\begin{bmatrix}1&T&0&0&0&0\\0&1&0&0&0&0\\0&0&1&T&0&0\\0&0&0&1&0&0\\0&0&0&0&1&T\\0&0&0&0&0&1\end{bmatrix} \tag{3}$$

and

$$\boldsymbol{F}_k^{\mathrm{CT}}=\begin{bmatrix}1&\sin(\omega T)/\omega&0&-[1-\cos(\omega T)]/\omega&0&0\\0&\cos(\omega T)&0&-\sin(\omega T)&0&0\\0&[1-\cos(\omega T)]/\omega&1&\sin(\omega T)/\omega&0&0\\0&\sin(\omega T)&0&\cos(\omega T)&0&0\\0&0&0&0&1&T\\0&0&0&0&0&1\end{bmatrix}. \tag{4}$$

The process noise matrix $\boldsymbol{G}_k$ is

$$\boldsymbol{G}_k=\begin{bmatrix}T^3/3&T^2/2&0&0&0&0\\T^2/2&T&0&0&0&0\\0&0&T^3/3&T^2/2&0&0\\0&0&T^2/2&T&0&0\\0&0&0&0&T^3/3&T^2/2\\0&0&0&0&T^2/2&T\end{bmatrix}. \tag{5}$$

The distance measurement received by the USN node i or AUV at time k can be expressed as

$$\begin{aligned}Z_k^i&=h(\boldsymbol{X}_k)+v_k^i\\&=\sqrt{(x_k-x^i)^2+(y_k-y^i)^2+(z_k-z^i)^2}+v_k^i,\end{aligned} \tag{6}$$

where (x^i, y^i, z^i) is the position coordinate of sensor node i and v_k^i is the zero-mean Gaussian noise of node i with variance R.

2.2 TD-CEKF algorithm

The target tracking algorithms based on USNs can be divided into two types—centralized and distributed (Tang et al., 2024). With the inclusion of AUVs as nodes and fusion centers, their computing power is much higher than that of ordinary USN nodes, and AUVs can surface to replenish power after completing their tasks. Therefore, the centralized fusion method is more suitable for the scenario of joint tracking with AUVs and USNs.

As shown in Fig. 1, the dashed arrows represent measurement information, while the solid arrows indicate the motion of the target. When the sensor receives the measurement of the target at time $k-1$, the target has already moved for τ seconds. In other words, the measurement information received by the sensor

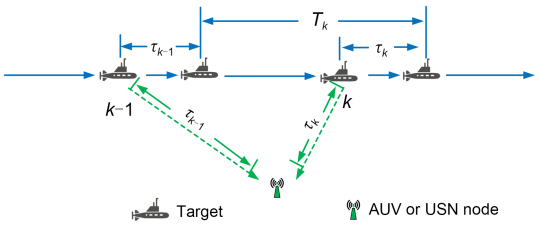

Fig. 1 Schematic diagram of measurement delay

corresponds to the target from τ seconds ago. This can lead to a discrepancy between the true position of the target and the measured position. This discrepancy is related to the transmission delay. The transmission delay is

$$\tau_i(\theta_i,\theta_{\mathrm{tg}})=-\frac{1}{\bar{a}}\left(\ln\frac{1+\sin\theta_{\mathrm{tg}}}{\cos\theta_{\mathrm{tg}}}-\ln\frac{1+\sin\theta_i}{\cos\theta_i}\right), \quad (7)$$

where θ_i and θ_{tg} represent the angles between the acoustic pulse and the horizontal plane at node i and the target, respectively, and $\bar{a}$ is the update coefficient (Zhao et al., 2021).

After obtaining the transmission delay, the predicted state is corrected to

$$\hat{\boldsymbol{X}}_{k+1|k}=\boldsymbol{F}\hat{\boldsymbol{X}}_k-\boldsymbol{\Lambda}_k, \quad (8)$$

where $\boldsymbol{\Lambda}_k$ is the delay correction vector, specifically:

$$\boldsymbol{\Lambda}_k=[\,\tau_k v_{x,k},0,\tau_k v_{y,k},0,\tau_k v_{z,k},0\,]^{\mathrm{T}}. \quad (9)$$

Thus, the corrected measurement residual is

$$\boldsymbol{Z}_{k+1}^{\mathrm{r}}=\boldsymbol{Z}_{k+1}-h\left(\boldsymbol{F}\hat{\boldsymbol{X}}_{k+1|k}-\boldsymbol{\Lambda}_k\right). \quad (10)$$

The Jacobian matrix is

$$\boldsymbol{H}_{k+1}=\frac{\partial h\left(\boldsymbol{F}\hat{\boldsymbol{X}}_{k+1|k}-\boldsymbol{\Lambda}_k\right)}{\partial\hat{\boldsymbol{X}}_{k+1|k}}=\begin{bmatrix}\frac{\hat{x}_{k+1}-x^1}{h\left(\hat{\boldsymbol{X}}_{k+1}\right)} & 0 & \frac{\hat{y}_{k+1}-y^1}{h\left(\hat{\boldsymbol{X}}_{k+1}\right)} & 0 & \frac{\hat{z}_{k+1}-z^1}{h\left(\hat{\boldsymbol{X}}_{k+1}\right)} & 0\\ \vdots & \vdots & \vdots & \vdots & \vdots & \vdots\\ \frac{\hat{x}_{k+1}-x^M}{h\left(\hat{\boldsymbol{X}}_{k+1}\right)} & 0 & \frac{\hat{y}_{k+1}-y^M}{h\left(\hat{\boldsymbol{X}}_{k+1}\right)} & 0 & \frac{\hat{z}_{k+1}-z^M}{h\left(\hat{\boldsymbol{X}}_{k+1}\right)} & 0\end{bmatrix}. \quad (11)$$

In summary, the process of the proposed TD-CEKF algorithm is shown in Algorithm 1.

Algorithm 1 Proposed TD-CEKF algorithm

1 Get the original measurement information
2 **for** i=1 to M **do**
3 Compute τ_i by Eq. (7)
4 **end for**
5 Correct the state prediction by Eq. (9)
6 Covariance forecasting: $\boldsymbol{P}_{k+1|k}=\boldsymbol{F}_k\boldsymbol{P}_k\boldsymbol{F}_k^{\mathrm{T}}+\boldsymbol{G}_k\boldsymbol{w}_k$
7 Calculate the Jacobian matrix using Eq. (11)
8 State update: $\hat{\boldsymbol{X}}_{k+1}=\hat{\boldsymbol{X}}_{k+1|k}+\boldsymbol{K}_{k+1}\boldsymbol{Z}_{k+1}^{\mathrm{r}}$
9 Covariance update: $\boldsymbol{P}_{k+1}=\boldsymbol{P}_{k+1|k}+\boldsymbol{K}_{k+1}\boldsymbol{H}_{k+1}\boldsymbol{P}_{k+1|k}$

3 Problem construction

In this section, the mathematical relationship between the AUV position and the FIM is derived, and the AUV position optimization problem is established using the AUV's movement range as a constraint.

3.1 Relationship between AUV position and FIM

According to Bayesian estimation theory, the mean square error of target state estimation cannot be lower than the Cramér–Rao lower bound (Teimouri and Hoseini, 2024; Yuan et al., 2024).

$$E\left\{\left[\hat{\boldsymbol{X}}_k-\boldsymbol{X}_k\right]\left[\hat{\boldsymbol{X}}_k-\boldsymbol{X}_k\right]^{\mathrm{T}}\right\}\geq\boldsymbol{J}_k^{-1}(\boldsymbol{X}_k), \quad (12)$$

where $\boldsymbol{J}_k^{-1}(\boldsymbol{X}_k)$ is the FIM and $\hat{\boldsymbol{X}}_k$ is the estimated state of the target. The $\boldsymbol{J}_k(\boldsymbol{X}_k)$ of the target at time k is expressed as

$$\boldsymbol{J}_k(\boldsymbol{X}_k)=-E_{p(\boldsymbol{Z}_k,\boldsymbol{X}_k|\boldsymbol{Z}_{1:k-1})}\left[\nabla_{\boldsymbol{X}_k}^{\boldsymbol{X}_k}\ln p(\boldsymbol{Z}_k,\boldsymbol{X}_k|\boldsymbol{Z}_{1:k-1})\right], \quad (13)$$

where $\nabla_{\boldsymbol{X}_k}^{\boldsymbol{X}_k}=\nabla_{\boldsymbol{X}_k}\nabla_{\boldsymbol{X}_k}^{\mathrm{T}}$ denotes the second-order partial derivative operator. $p(\boldsymbol{Z}_k,\boldsymbol{X}_k|\boldsymbol{Z}_{1:k-1})$ is the joint probability density of the measurement (Luo and Han, 2019), which can be decomposed into

$$p\left(\boldsymbol{Z}_k,\boldsymbol{X}_k|\boldsymbol{Z}_{1:k-1}\right)=p\left(\boldsymbol{Z}_k|\boldsymbol{X}_k\right)p\left(\boldsymbol{X}_k|\boldsymbol{Z}_{1:k-1}\right). \quad (14)$$

Therefore, $\boldsymbol{J}_k(\boldsymbol{X}_k)$ can be decomposed into

$$\boldsymbol{J}_k(\boldsymbol{X}_k)=\boldsymbol{J}_k^{\mathrm{p}}(\boldsymbol{X}_k)+\boldsymbol{J}_k^{\mathrm{s}}(\boldsymbol{X}_k), \quad (15)$$

where $\boldsymbol{J}_k^{\mathrm{p}}(\boldsymbol{X}_k)$ is related to prior information and $\boldsymbol{J}_k^{\mathrm{s}}(\boldsymbol{X}_k)$ is related to predictive data. The specific calculation methods (Shi et al., 2021) are as follows:

$$\boldsymbol{J}_k^{\mathrm{p}}(\boldsymbol{X}_k)=-E_{p(\boldsymbol{X}_k|\boldsymbol{Z}_{1:k-1})}\left[\nabla_{\boldsymbol{X}_k}^{\boldsymbol{X}_k}\ln p\left(\boldsymbol{X}_k|\boldsymbol{Z}_{1:k-1}\right)\right]\approx\sum_{\boldsymbol{X}_k}^{-1}, \quad (16)$$

$$\boldsymbol{J}_k^{\mathrm{s}}(\boldsymbol{X}_k)=-E_{p(\boldsymbol{Z}_k|\boldsymbol{X}_k)}\left[\nabla_{\boldsymbol{X}_k}^{\boldsymbol{X}_k}\ln p\left(\boldsymbol{Z}_k|\boldsymbol{X}_k\right)\right]=\boldsymbol{D}_k^{\mathrm{T}}\sum_{\boldsymbol{Z}_k}^{-1}\boldsymbol{D}_k, \quad (17)$$

where $\sum_{\boldsymbol{X}_k}$ is the error covariance matrix, $\sum_{\boldsymbol{Z}_k}$ is the measurement noise matrix, and $\boldsymbol{D}_k=\left[\nabla_{\boldsymbol{X}_k}h(\boldsymbol{X}_k)\right]^{\mathrm{T}}$ is the Jacobian matrix. Therefore, the relationship between AUV position $\boldsymbol{u}=(x^{\mathrm{A}}, y^{\mathrm{A}}, z^{\mathrm{A}})$ and the FIM is

$$\begin{aligned}&\boldsymbol{J}_k(\boldsymbol{X}_k,\boldsymbol{u})\\&=\boldsymbol{J}_k^{\mathrm{p}}(\boldsymbol{X}_k,\boldsymbol{u})+\boldsymbol{J}_k^{\mathrm{s}}(\boldsymbol{X}_k,\boldsymbol{u})\\&=\sum_{\boldsymbol{X}_k}^{-1}+\boldsymbol{D}_k^{\mathrm{T}}\sum_{\boldsymbol{Z}_k}^{-1}\boldsymbol{D}_k\\&=\sum_{\boldsymbol{X}_k}^{-1}+\frac{1}{h^2(\boldsymbol{X}_k^{\mathrm{A}})R}\begin{bmatrix}A^2&0&AB&0&AC&0\\0&0&0&0&0&0\\BA&0&B^2&0&BC&0\\0&0&0&0&0&0\\CA&0&CB&0&C^2&0\\0&0&0&0&0&0\end{bmatrix},\end{aligned} \quad (18)$$

where $A=x_k-x^{\mathrm{A}}$, $B=y_k-y^{\mathrm{A}}$, and $C=z_k-z^{\mathrm{A}}$. The state $\boldsymbol{X}_k$ of the target is always unknown in the tracking process, so here, $\boldsymbol{X}_k$ is replaced by the estimated state $\hat{\boldsymbol{X}}_k$.

3.2 AUV position optimization problem construction

According to the mathematical relationship between the AUV position and the FIM, the change in the AUV position affects the lower bound of target state estimation. The displacement vector of the AUV in the 3D space is assumed to be $\Delta\boldsymbol{u}=(\Delta x^{\mathrm{A}}, \Delta y^{\mathrm{A}}, \Delta z^{\mathrm{A}})$; thus, the FIM at time k can be expressed as a function of the displacement vector $\boldsymbol{J}_k(\boldsymbol{X}_k, \boldsymbol{u}+\Delta\boldsymbol{u})$ and the predicted value $\boldsymbol{X}_k$. For each tracking time step, the predicted value remains unchanged after the data fusion is completed, so the FIM is related only to the displacement vector. By selecting the AUV displacement vector for the next moment, the FIM can be increased, which is equivalent to reducing the lower bound of the mean square estimation error. Therefore, the objective function of the AUV position optimization problem is constructed as follows:

$$\begin{aligned}&\arg\max_{\Delta\boldsymbol{u}}\lg\det\left[\boldsymbol{J}_k(\Delta\boldsymbol{u})\right]\\&\text{s.t.}\begin{cases}\left|\Delta x^{\mathrm{A}}\right|\le v_xT,\\\left|\Delta y^{\mathrm{A}}\right|\le v_yT,\\\left|\Delta z^{\mathrm{A}}\right|\le v_zT,\end{cases}\end{aligned} \quad (19)$$

where v_x, v_y, and v_z are the velocity components of the AUV in the 3D space. The constraint is the maximum distance that the AUV can move within the sampling interval (e.g., AUV speed v multiplied by the sampling interval T). For ease of calculation, the AUV's speed is decomposed into 3D components. For the FIM, the D-criterion is used in this paper (Moreno-Salinas et al., 2013), and the logarithm of the determinant value of FIM is used to facilitate the solution process later.

4 Solution of AUV position

In this section, the Lagrange multiplier method is used to remove the constraints from the objective function, and the optimal position of the AUV is solved using the gradient descent method.

Eq. (18) has been proven to be a convex problem (Zhang ZK et al., 2023). Due to the relatively simple form of function (19) and the high real-time requirements for target tracking, the gradient descent method is employed in this paper, which has a high search efficiency. The problem needs to be unconstrained first. The unconstrained objective function can be constructed using the penalty function method:

$$\begin{aligned}\psi(\Delta\boldsymbol{u},\zeta)=&-\lg\det\left[\boldsymbol{J}_k(\Delta\boldsymbol{u})\right]-\zeta[\lg(v_xT-\Delta x^{\mathrm{A}})\\&+\lg(v_xT+\Delta x^{\mathrm{A}})+\lg(v_yT-\Delta y^{\mathrm{A}})\\&+\lg(v_yT+\Delta y^{\mathrm{A}})+\lg(v_zT-\Delta z^{\mathrm{A}})\\&+\lg(v_zT+\Delta z^{\mathrm{A}})],\end{aligned} \quad (20)$$

where ζ is the penalty factor. Since the gradient descent method is used, the objective function is negative in Eq. (20), and the maximization problem is transformed into a minimization problem.

According to the property $\frac{\partial\lg\det(\boldsymbol{Q})}{\partial q}=\mathrm{tr}\left[\boldsymbol{Q}^{-1}\frac{\partial\boldsymbol{Q}}{\partial q}\right]$, the gradient of $\psi(\Delta\boldsymbol{u}, \zeta)$ is

$$\nabla_{\Delta \boldsymbol{u}}\psi(\Delta\boldsymbol{u},\zeta)=[\nabla_{\Delta x}\psi(\Delta x^{\mathrm{A}},\zeta),\nabla_{\Delta y}\psi(\Delta y^{\mathrm{A}},\zeta),\nabla_{\Delta z}\psi(\Delta z^{A},\zeta)], \quad (21)$$

where $\nabla_{\Delta x}\psi(\Delta x^{\mathrm{A}},\zeta)$ is written as Eq. (22) (at the bottom of this page).

Similarly, we can obtain

$$\nabla_{\Delta y}\psi(\Delta y^{\mathrm{A}},\zeta)=-\mathrm{tr}\left[\boldsymbol{J}_k^{-1}(\Delta\boldsymbol{u})\frac{\partial \boldsymbol{J}_k(\Delta\boldsymbol{u})}{\partial \Delta y^{\mathrm{A}}}\right]-\zeta\left(\frac{1}{v_yT-\Delta y^{\mathrm{A}}}+\frac{1}{v_yT+\Delta y^{\mathrm{A}}}\right), \quad (23)$$

$$\nabla_{\Delta z}\psi(\Delta z^{\mathrm{A}},\zeta)=-\mathrm{tr}\left[\boldsymbol{J}_k^{-1}(\Delta\boldsymbol{u})\frac{\partial \boldsymbol{J}_k(\Delta\boldsymbol{u})}{\partial \Delta z^{\mathrm{A}}}\right]-\zeta\left(\frac{1}{v_zT-\Delta z^{\mathrm{A}}}+\frac{1}{v_zT+\Delta z^{\mathrm{A}}}\right). \quad (24)$$

After the gradient vector is obtained, the gradient descent method can be used to search. The overall search process is shown in Algorithm 2.

Algorithm 2 AUV position search algorithm

Select the initial value, set $\zeta>0$, $\eta>1$, $k=1$, $L=0$, $0\le\varepsilon_1\le1$, $0\le\varepsilon_2\le1$, and $\vartheta\in(0,1)$

1 Calculate gradient $g_L=-\nabla_{\Delta \boldsymbol{u}}\psi(\Delta\boldsymbol{u},\zeta)$

2 If $|g_L|\le\varepsilon_1$, then $\Delta\boldsymbol{u}_k^*=\Delta\boldsymbol{u}_L$; go to line 6

3 Use the linear backtracking method to determine the step length α_L

4 Let $\Delta\boldsymbol{u}_L=\Delta\boldsymbol{u}_L+\alpha_L g_L$

5 Let $L=L+1$; go to line 1

6 If $\zeta H(\boldsymbol{u})\le\varepsilon_2$, then output $\Delta\boldsymbol{u}^*=\Delta\boldsymbol{u}_k$; otherwise, go to line 7

7 Let $\sigma_{k+1}=\eta\sigma_k$

8 Let $k=k+1$; go to line 1

$H(\boldsymbol{u})$ represents the augmented part of the objective function. Combined with the above, the overall flowchart is shown in Fig. 2. The USN nodes and the AUV first receive the measurement echo, and then each USN node transmits the measurement value to the AUV. The measurement data have a flag bit so that the AUV can distinguish the source of the measurement value. Upon acquiring the measurement data, the AUV executes Algorithm 1 to obtain the target's predicted state, followed by executing Algorithm 2 to determine the AUV's new position coordinates and initiate movement. This process is repeated at each subsequent time step until the tracking task is completed. After each movement, the AUV checks if it has sufficient energy to complete the next tracking operation. If not, it will return to the surface for recharging. After this, the USN nodes will continue to carry out the tracking task.

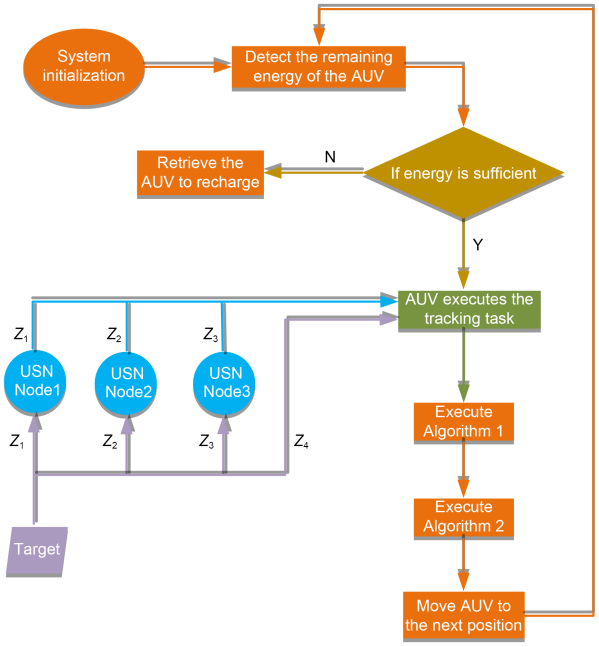

Fig. 2 Flowchart of the proposed joint tracking

$$\nabla_{\Delta x}\psi(\Delta x^{\mathrm{A}},\zeta)=-\mathrm{tr}\left[\boldsymbol{J}_k^{-1}(\Delta\boldsymbol{u})\frac{\partial \boldsymbol{J}_k(\Delta\boldsymbol{u})}{\partial \Delta x^{\mathrm{A}}}\right]-\zeta\left(\frac{1}{v_xT-\Delta x^{\mathrm{A}}}+\frac{1}{v_xT+\Delta x^{\mathrm{A}}}\right)$$

$$=-\mathrm{tr}\left\{\boldsymbol{J}_k^{-1}(\Delta x^{\mathrm{A}})\left[\boldsymbol{J}_k^{\mathrm{U}}\frac{2(v_k-\Delta x^{\mathrm{A}})}{Rh^3(X_k^{\mathrm{A}})}+\frac{1}{Rh^2(X_k^{\mathrm{A}})}\begin{bmatrix}-2(x_k-\Delta x^{\mathrm{A}}) & 0 & -(y_k-\Delta y^{\mathrm{A}}) & 0 & -(z_k-\Delta z^{\mathrm{A}}) & 0\\ 0 & 0 & 0 & 0 & 0 & 0\\ -(y_k-\Delta y^{\mathrm{A}}) & 0 & 0 & 0 & 0 & 0\\ 0 & 0 & 0 & 0 & 0 & 0\\ -(z_k-\Delta z^{\mathrm{A}}) & 0 & 0 & 0 & 0 & 0\\ 0 & 0 & 0 & 0 & 0 & 0\end{bmatrix}\right]\right\}. \quad (22)$$

5 Simulations and analysis

In this section, simulations are conducted to validate the effectiveness of the proposed algorithm. The parameters are set as follows: the tracking duration is 50 s, the sampling interval T is 1 s, the covariance of measurement noise R is 5, and the process noise variance coefficient $q^2=10^{-2}$. The target motion follows a CT model with a turning speed ω of 0.15 rad/s, and the underwater acoustic signal propagation speed is 1473 m/s. The initial state of the target is $\boldsymbol{X}_1=[150, 5, 100, 5, 32, 5]^{\mathrm{T}}$, the initial estimated state is $\hat{\boldsymbol{X}}_1=[151, 5, 98, 5, 32, 5]^{\mathrm{T}}$, and the update coefficient $\bar{a}=0.017$. In the first part of the simulation, four underwater sensor nodes are set. Their coordinates are (40, 10, 10), (70, 80, 80), (65, 70, 40), and (60, 90, 20).

The setting parameters of the tracking scenarios are summarized in Table 1. In this paper, the root mean square error (RMSE) of the target state estimation is used as an accuracy measure of state estimation. At time k, the RMSE of the estimation $\hat{\boldsymbol{X}}_k$ of the target state $\boldsymbol{X}_k$ is

$$\mathrm{RMSE}_k=\sqrt{\sum_{i=1}^{\mathrm{MC}}\frac{\left\|\boldsymbol{X}_k-\hat{\boldsymbol{X}}_k\right\|^2}{\mathrm{MC}}}, \tag{25}$$

where MC is the number of Monte Carlo simulations. To avoid contingency, all simulations in this paper are conducted 200 times.

Table 1 Parameters used for the simulations

Parameter	Value
Sampling interval T (s)	1
Tracking duration (s)	50
Covariance of measurement noise R	5
Intensity of process noise q^2	10^{-2}
Turning speed ω (rad/s)	0.15
Underwater acoustic signal propagation speed c (m/s)	1473
Update coefficient $\bar{a}$	0.017
Monitored field (m×m×m)	200×100×600
Initial position of the target	(150, 100, 32)
AUV navigation speed v (m/s)	5
Number of USN nodes	4

The first simulation involves the TD-CEKF algorithm proposed in Section 2. The comparison algorithms are the time offset estimation UKF (TO-UKF) fusion algorithm (Su et al., 2020) and the improved time delay estimation particle filter (TD-PF) algorithm (Zhang ZK et al., 2023). The two particle filter algorithms use a sequential importance resampling (SIR) particle filter; to fully verify the effectiveness of the algorithms, the number of particles is set to 1000. Fig. 3 shows the comparison of the estimated path of each algorithm for target tracking. Compared with the estimated paths of the TO-UKF and TD-PF algorithms, the estimated path obtained by this algorithm is closer to the true path of target motion.

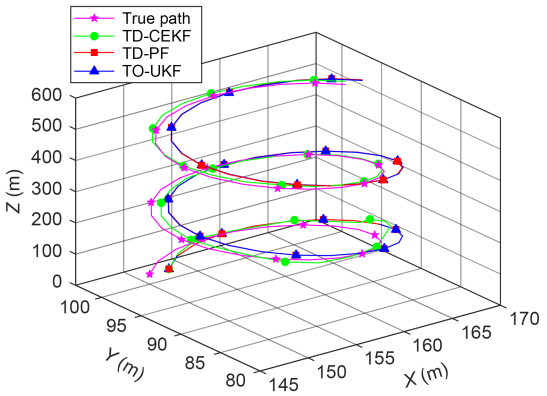

Fig. 3 Underwater tracking scene

Figs. 4a and 4b show the transmission delay τ at different target speeds and the target position deviation caused by τ at different target speeds. The velocity vectors are $[1, 1, 1]^{\mathrm{T}}$, $[2, 2, 2]^{\mathrm{T}}$, and $[3, 3, 3]^{\mathrm{T}}$. In Fig. 4a, the larger the target's velocity is, the greater the transmission delay τ becomes. Eq. (7) shows that τ is related to the angles between the acoustic pulse and the horizontal plane at the node and the target. The greater the velocity of the target, the greater the horizontal angle of the ranging acoustic pulse of node 1 at the target, so the greater the τ. Over time, although τ moves up and down, the overall trend increases. This is because the turning speed of the target under CT motion is relatively large, and the radius is only 10 m, which is far less than the range of the target rising. In general, the target is constantly away from node 1. Therefore, the τ of the acoustic pulse echo increases. In addition, when the sensor is about 250 m away from the target, the combined speed of the velocity components in

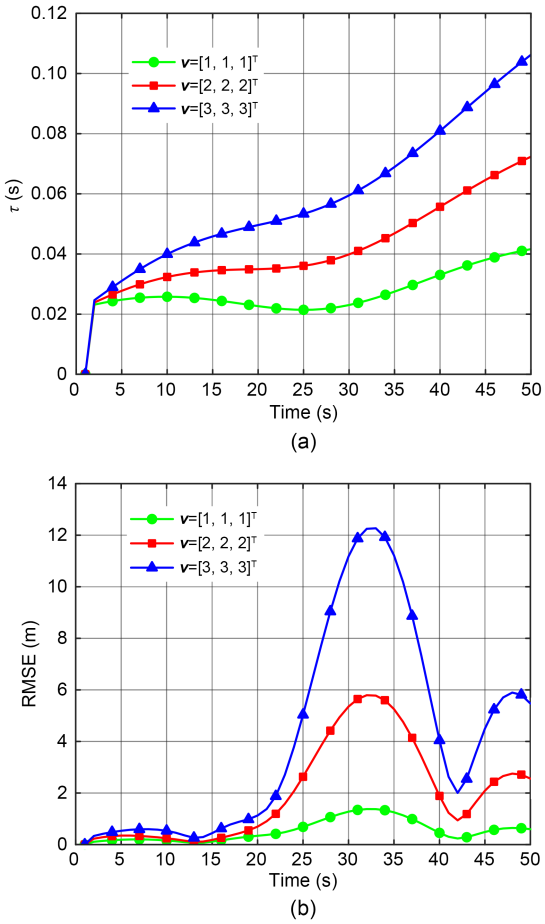

Fig. 4 Comparison of transmission delay τ (a) and the root mean square error (RMSE) of the position deviation (b) at different target speeds

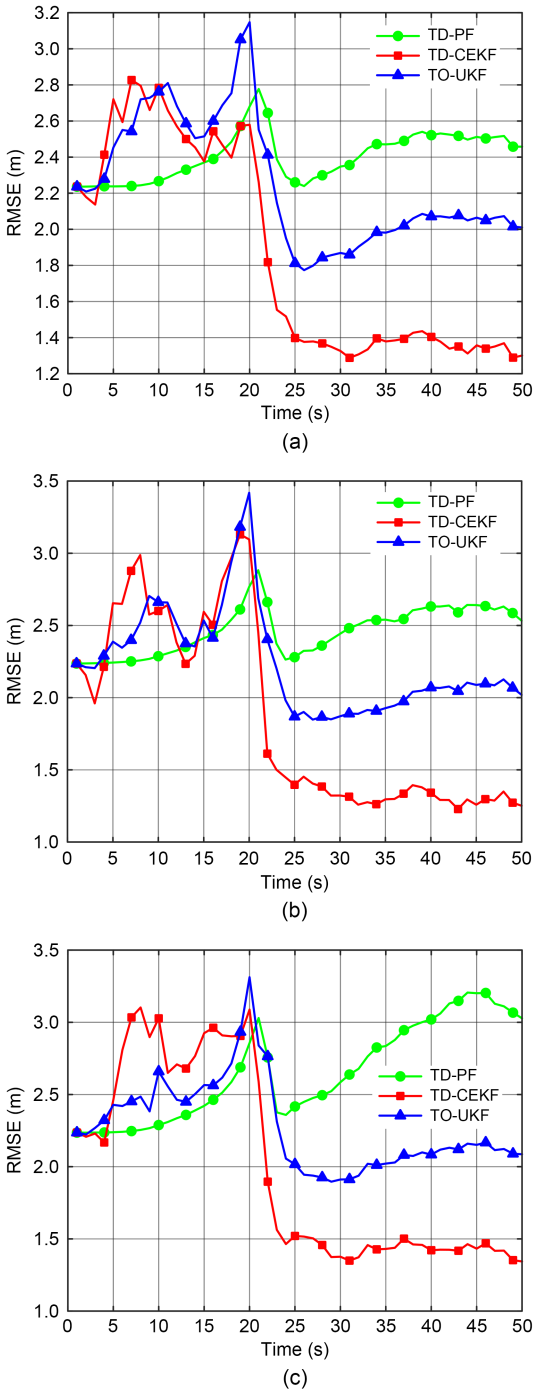

Fig. 5 RMSE comparison of time delay estimation algorithms under v=[5, 5, 5]^{T} (a), v=[7, 7, 7]^{T} (b), and v=[9, 9, 9]^{T} (c)

each dimension is 40 m/s, and τ is about 0.2 s, which is far less than that during the sampling period, and the speed of the underwater target is generally not higher than 40 knots (20.57 m/s). When the speed of the target becomes higher, τ constantly increases, resulting in an increase in the RMSE of the position deviation in Fig. 4b. Notably, the trend of τ in Fig. 4a is inconsistent with the RMSE of the position deviation in Fig. 4b because Fig. 4a shows only the time delay change of USN node 1, while Fig. 4b represents the RMSE calculated from all USN nodes' time delays.

Fig. 5 compares the RMSE of each time delay estimation fusion algorithm. The velocity vector of the target in Fig. 5a is [5, 5, 5]^{T}. The tracking accuracy of the TD-PF algorithm is better than that of the TO-UKF algorithm and the proposed TD-CEKF algorithm at the beginning of the tracking task. However, as the tracking task progresses, the RMSE of each algorithm begins to rise, and a huge jitter occurs. When the tracking of each algorithm is stabilized, the proposed TD-CEKF algorithm shows its advantages. From the 20th time step onward, the RMSE of TD-CEKF algorithm is lower than that of the other two algorithms, and it remains stable between 1.2 m and 1.5 m. The

RMSE of the TO-UKF algorithm in this scenario is lower than that of the TD-PF algorithm. This is because the TO-UKF algorithm is less prone to particle degeneracy issues, making it more accurate in the particle approximation of transmission delay. The TD-CEKF algorithm has more advantages in time delay estimation by integrating global information.

The velocity vectors of the target in Figs. 5b and 5c are $[7, 7, 7]^{\mathrm{T}}$ and $[9, 9, 9]^{\mathrm{T}}$, respectively. In Fig. 5b, the proposed TD-CEKF algorithm still has a better tracking effect than the other algorithms. The TO-UKF algorithm begins to show advantages in the time delay estimation of unscented particles when the speed is large, and its tracking RMSE is better than that of the TD-PF algorithm; however, there is still a certain gap with the proposed TD-CEKF algorithm. The RMSE gap of each algorithm in Fig. 5c is larger than that in Figs. 5a and 5b, and the proposed TD-CEKF algorithm still achieves the best tracking performance. Comparing these three diagrams in Fig. 5, the TD-PF algorithm estimates the transmission delay through many particle approximations, but the particle degradation phenomenon of the particle filter makes the estimation of the delay inaccurate. The TO-UKF algorithm introduces the transmission delay into the sigma particle of the unscented transformation, but the unscented transformation has a serious dependence on the accuracy of the initial value estimation, so the performance is not as good as that of the proposed TD-CEKF algorithm when there is an initial error. The proposed TD-CEKF algorithm can achieve better tracking results than the estimation algorithm of particle simulation by introducing time delay correction to the centralized Jacobian matrix.

Fig. 6a shows the comparison of the execution times of the three time delay fusion algorithms. The operating environment is an Intel® Core™ i9-13900H central processing unit (CPU) running at 2.60 GHz. For convenience of display, Fig. 6a shows the results after taking the logarithm of the execution time of each algorithm. Neither the TD-CEKF algorithm nor the TO-UKF algorithm requires many particles to estimate the delay approximately, so the order of magnitude of the execution time at each time step is much smaller than that of the TD-PF algorithm. It is worth noting that in Fig. 6a, the order of magnitude of the execution time of the TD-CEKF and TO-UKF algorithms

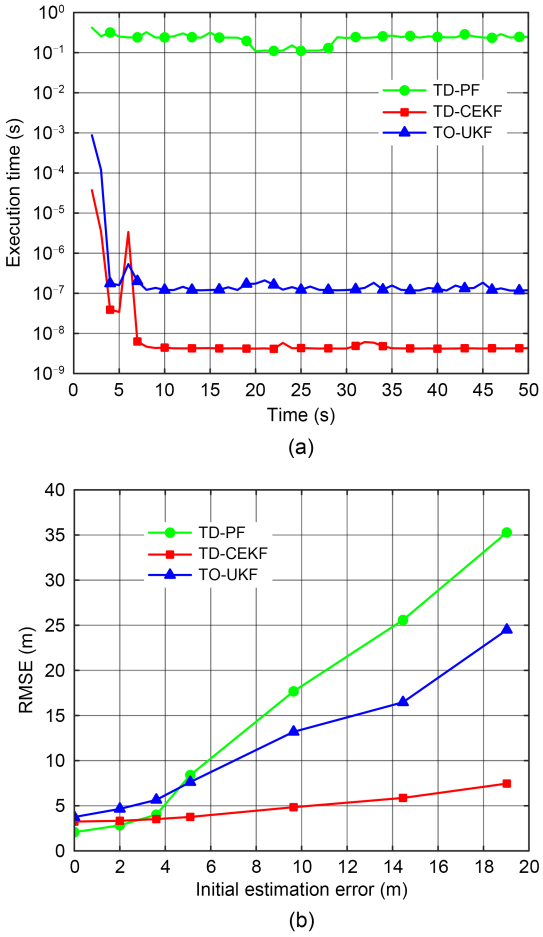

Fig. 6 Comprehensive comparison of time delay estimation algorithms: (a) comparison of the execution time; (b) RMSE under different initial estimation errors

is much smaller than that of the TD-PF algorithm, reaching 10^{-6} s when running on a computer. If running on the CPU of the sensor node, the time consumed will be much greater than 10^{-6} s. In practical engineering applications, the time delay estimation algorithm based on the particle filter and unscented transformation has higher requirements on the computing power of the CPU, which makes it difficult to meet engineering application requirements.

Fig. 6b shows the average tracking RMSE comparison of each algorithm under different initial estimation errors. The abscissa is a different initial estimation error. The TD-CEKF algorithm is less affected by the initial estimation error, while the TO-UKF and TD-PF algorithms are greatly affected by the initial state. This is because the particle approximation requires high accuracy of the initial estimated state.

However, in a complex underwater environment, the initial estimation error is not low.

Therefore, by comprehensively comparing the RMSE and execution time of each algorithm, the TD-CEKF algorithm is more suitable for application in the field of complex underwater target tracking.

For the AUV position search algorithm proposed in this paper, the simulation is set as follows: the tracking duration is 100 time steps. The motion of the target remains CT motion, as shown in Fig. 3, with a turning speed of 0.15 rad/s. This section compares scenarios where four USN nodes participate in tracking. The positions of the three nodes remain consistent under both the traditional USN-based tracking algorithm and the AUV–USN cooperative tracking algorithm proposed in this paper. To verify the influence of AUV on the topology, both adopt the TD-CEKF algorithm.

Figs. 7–9 compare the tracking RMSE and posterior Cramér–Rao lower bound (PCRLB) under different process noises. The variance coefficient of the process noise in Fig. 7 is $q^2=10^{-4}$. Compared with ordinary USNs, after replacing an ordinary USN node with an AUV, the AUV continuously changes its position according to the proposed algorithm to form a better topology, so the tracking accuracy is significantly higher than that of ordinary USNs. In addition, the joint tracking by AUV and USN nodes is more stable in terms of tracking stability. The RMSE gradually stabilizes after the 30th time step, while the tracking RMSE of the USN fluctuates greatly due to the fixation of nodes.

Fig. 7b more intuitively illustrates the performance of the AUV location search algorithm proposed in this paper. At each time step, the AUV moves to a

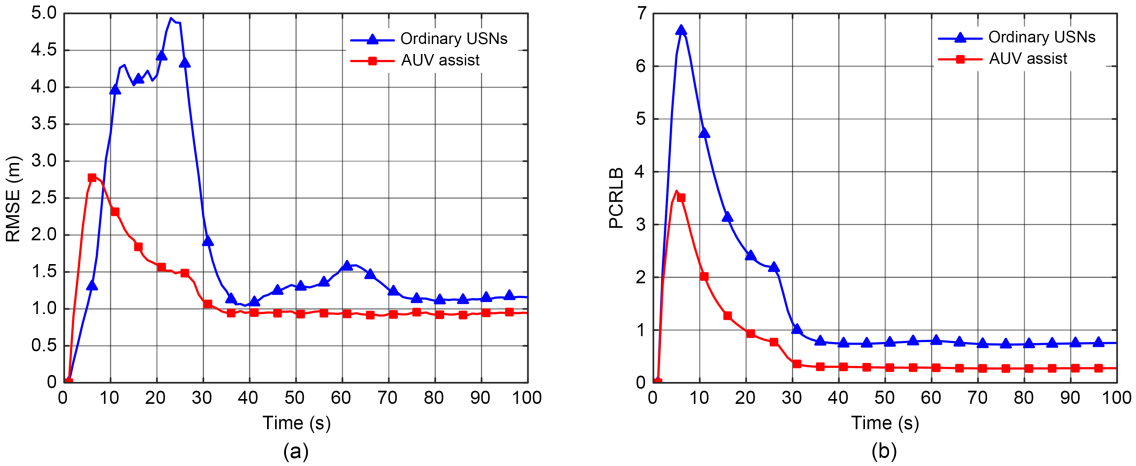

Fig. 7 Comparison of tracking performance before and after optimization ($q^2=10^{-4}$): (a) RMSE; (b) PCRLB

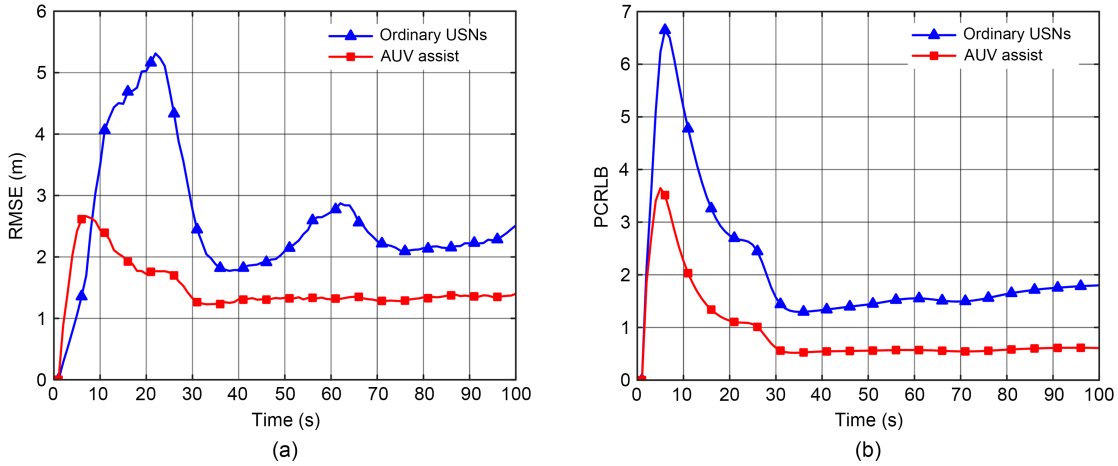

Fig. 8 Comparison of tracking performance before and after optimization ($q^2=10^{-3}$): (a) RMSE; (b) PCRLB

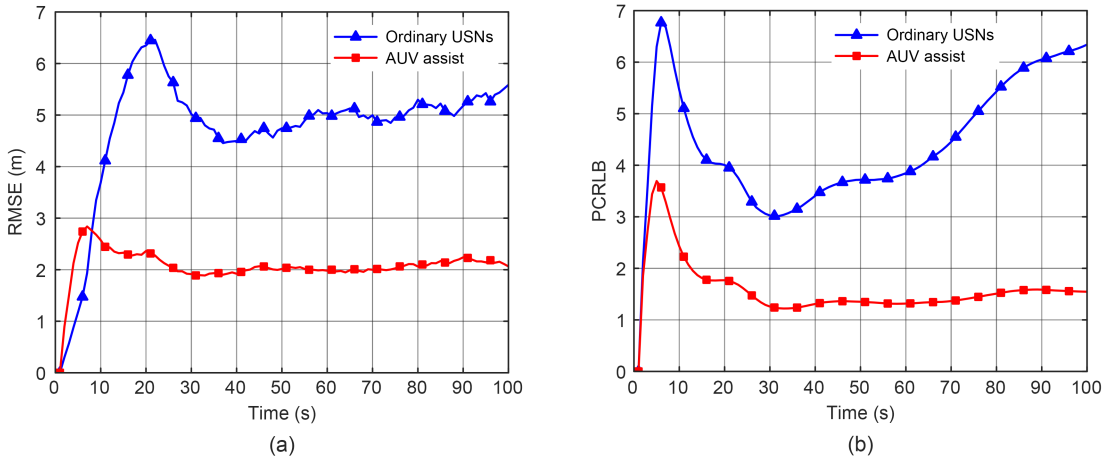

Fig. 9 Comparison of tracking performance before and after optimization (q^2=10^{-2}): (a) RMSE; (b) PCRLB

location with a larger FIM (i.e., a position with a smaller PCRLB). Therefore, the PCRLB value after the AUV position moves in Fig. 7b is smaller than that of the topology composed of ordinary USN nodes. The process noise variance coefficients in Figs. 8 and 9 are q^2=10^{-3} and q^2=10^{-2}, respectively. A longitudinal comparison of these three sets of maps reveals that with the continuous increase in process noise, both tracking methods are affected to varying degrees, and the RMSE and PCRLB increase. However, the tracking based on USN fixed nodes is obviously affected by noise. When the process noise variance coefficient q^2 increases from 10^{-4} to 10^{-2}, the RMSE correspondingly increases from about 1.15 m to about 5 m. The joint tracking method of AUV and USN nodes is less disturbed by noise because the AUV is constantly moving to the larger position of FIM, and the RMSE increases slightly from 0.92 m at q^2=10^{-4} to about 2 m at q^2=10^{-2}, which is much smaller than the tracking growth rate based on USN fixed nodes. It can also be seen from the comparison of the PCRLB results that the proposed joint tracking method in this paper has stronger noise immunity performance. In the actual underwater environment, the noise and reverberation in the underwater acoustic channel are far more serious than those in the land environment. Therefore, the method based on AUV and USN joint tracking is more suitable for underwater target tracking.

Fig. 10 presents a comparison of execution times of the two tracking methods. Tracking based on fixed USN nodes has, on average, a shorter execution time, as it does not require a search algorithm. In contrast,

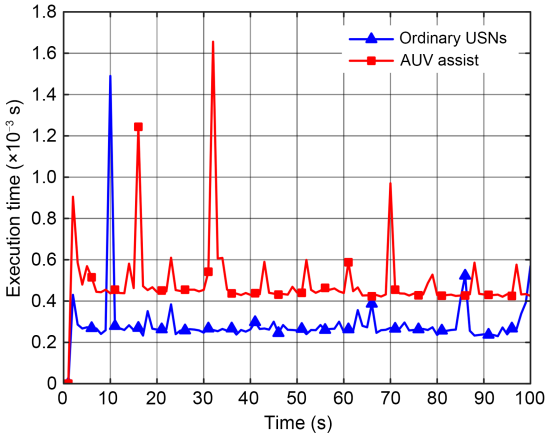

Fig. 10 Comparison of algorithm execution time

the execution time of the joint tracking algorithm involving the AUV and USN is greater due to the need for a gradient descent search for the AUV position. However, as shown in Fig. 10, the additional time required for searching the AUV position is relatively small, keeping the execution times of both methods within the same order of magnitude and not significantly different. The proposed AUV and USN joint tracking algorithm is capable of underwater target tracking. Furthermore, since the AUV acts as the fusion center, it reduces the number of sensor nodes involved in tracking and their computational tasks, thereby saving energy and extending the lifespan of the entire sensor network. Unavoidably, the deployment and operation of AUVs incur costs and energy consumption. However, this is worthwhile compared to the high cost and extremely limited and non-recoverable energy resources

of USN nodes. In addition, in the joint tracking algorithm proposed in this paper, the AUV tracking method is based on hydrophone ranging, which is significantly more cost-effective than the traditional sonar imaging tracking methods used in AUVs.

6 Conclusions

Underwater target tracking using USNs currently faces challenges such as limited energy and underwater acoustic transmission delay. To address these issues, first, the influence of transmission delay on target tracking is effectively mitigated by the proposed TD-CEKF algorithm. Second, a joint tracking method using both AUV and USN nodes is introduced, which results in better tracking accuracy and noise immunity performance compared to tracking solely using USN nodes. Finally, the simulation results demonstrate that the proposed joint tracking algorithm not only reduces the task load of the USN nodes during underwater target tracking but also achieves improved tracking performance. In future work, we will focus on AUV position optimization with multiple targets and evaluate how asynchronous sensor timing affects tracking.

Contributors

Zhaohong LV designed the research. All the authors performed the simulations. Zhenkai ZHANG and Yi YANG drafted the paper. Boon-Chong SEET revised the paper. All the authors read and approved the final version.

Conflict of interest

All the authors declare that they have no conflict of interest.

Data availability

The data that support the findings of this study are available from the corresponding author upon reasonable request.

References

Alostad JM, 2020. Reliability in IoUT enabled underwater sensor networks using dynamic adaptive routing protocol. *Int J Int Manuf Serv*, 7(1-2):115-129. https://doi.org/10.1504/IJIMS.2020.105041

Chen B, Hu JP, Zhao YY, et al., 2022a. Finite-time observer based tracking control of uncertain heterogeneous underwater vehicles using adaptive sliding mode approach. *Neurocomputing*, 481:322-332. https://doi.org/10.1016/j.neucom.2022.01.038

Chen B, Hu JP, Zhao YY, et al., 2022b. Finite-time velocity-free rendezvous control of multiple AUV systems with intermittent communication. *IEEE Trans Syst Man Cybern Syst*, 52(10):6618-6629. https://doi.org/10.1109/TSMC.2022.3148295

Jahanbakht M, Xiang W, Hanzo L, et al., 2021. Internet of Underwater Things and big marine data analytics—a comprehensive survey. *IEEE Commun Surv Tutor*, 23(2):904-956. https://doi.org/10.1109/COMST.2021.3053118

Li YD, Zhuang HC, Xu L, et al., 2025. Hierarchical detection and tracking for moving targets in underwater wireless sensor networks. *Digit Commun Netw*, 11(2):556-562. https://doi.org/10.1016/j.dcan.2024.03.008

Luo JH, Han Y, 2019. A node depth adjustment method with computation-efficiency based on performance bound for range-only target tracking in UWSNs. *Signal Process*, 158: 79-90. https://doi.org/10.1016/j.sigpro.2018.12.014

Luo JH, Han Y, He XT, 2019. Optimal bit allocation for maneuvering target tracking in UWSNs with additive and multiplicative noise. *Signal Process*, 164:125-135. https://doi.org/10.1016/j.sigpro.2019.06.005

Mohsan SAH, Mazinani A, Othman NQH, et al., 2022. Towards the internet of underwater things: a comprehensive survey. *Earth Sci Inform*, 15(2):735-764. https://doi.org/10.1007/s12145-021-00762-8

Moreno-Salinas D, Pascoal A, Aranda J, 2013. Sensor networks for optimal target localization with bearings-only measurements in constrained three-dimensional scenarios. *Sensors*, 13(8):10386-10417. https://doi.org/10.3390/s130810386

Shi YC, Jiu B, Yan JK, et al., 2021. Data-driven simultaneous multibeam power allocation: when multiple targets tracking meets deep reinforcement learning. *IEEE Syst J*, 15(1): 1264-1274. https://doi.org/10.1109/JSYST.2020.2984774

Song SS, Liu J, Guo JN, et al., 2023. Efficient data collection scheme for multi-modal underwater sensor networks based on deep reinforcement learning. *IEEE Trans Veh Technol*, 72(5):6558-6570. https://doi.org/10.1109/TVT.2022.3232391

Su J, Li YA, Ali W, 2020. Underwater angle-only tracking with propagation delay and time-offset between observers. *Signal Process*, 176:107581. https://doi.org/10.1016/j.sigpro.2020.107581

Tang MY, Liu MQ, Zhang SL, et al., 2024. Distributed target tracking in UWSNs under stochastic node communication scheme. *IEEE Sens J*, 24(3):3912-3926. https://doi.org/10.1109/JSEN.2023.3342090

Teimouri M, Hoseini SM, 2024. Observed Fisher information for radar clutter modeled with sub-Gaussian α-stable distribution. *Digit Signal Process*, 146:104382. https://doi.org/10.1016/j.dsp.2024.104382

Tian SK, Zhang ZK, 2021. Tracking energy control algorithm based on underwater sensor networks assisted by AUV. Int Conf on Autonomous Unmanned Systems, p.379-388. https://doi.org/10.1007/978-981-16-9492-9_38

Tian SK, Zhang ZK, 2022. A node selection algorithm based on multi-objective optimization under position floating. *IEEE Access*, 10:41863-41873.

https://doi.org/10.1109/ACCESS.2022.3167642

Wang LL, Xu XY, An SM, et al., 2024. CodeUNet: autonomous underwater vehicle real visual enhancement via underwater codebook priors. *ISPRS J Photogramm Remote Sens*, 215:99-111. https://doi.org/10.1016/j.isprsjprs.2024.06.009

Xu B, Guo Y, 2022. A novel DVL calibration method based on robust invariant extended Kalman filter. *IEEE Trans Veh Technol*, 71(9):9422-9434. https://doi.org/10.1109/TVT.2022.3182017

Xu B, Wang XY, Zhang J, et al., 2022. A novel adaptive filtering for cooperative localization under compass failure and non-Gaussian noise. *IEEE Trans Veh Technol*, 71(4):3737-3749. https://doi.org/10.1109/TVT.2022.3145095

Yuan Y, Liu XY, Li WJ, et al., 2024. Decentralized resource allocation for multi-radar systems based on quality of service framework. *IEEE Trans Signal Process*, 72:1189-1204. https://doi.org/10.1109/TSP.2024.3367278

Zhang D, Liu MQ, Zhang SL, et al., 2018. Mutual-information based weighted fusion for target tracking in underwater wireless sensor networks. *Front Inform Technol Electron Eng*, 19(4):544-556. https://doi.org/10.1631/FITEE.1601695

Zhang D, Liu MQ, Zhang SL, et al., 2019. Non-myopic energy allocation for target tracking in energy harvesting UWSNs. *IEEE Sens J*, 19(10):3772-3783. https://doi.org/10.1109/JSEN.2018.2890078

Zhang JX, Liu MQ, Zhang SL, et al., 2022. Robust global route planning for an autonomous underwater vehicle in a stochastic environment. *Front Inform Technol Electron Eng*, 23(11):1658-1672. https://doi.org/10.1631/FITEE.2200026

Zhang Q, Liu MQ, Zhang SL, 2015. Node topology effect on target tracking based on UWSNs using quantized measurements. *IEEE Trans Cybern*, 45(10):2323-2335. https://doi.org/10.1109/TCYB.2014.2371232

Zhang SL, Chen HY, Liu MQ, et al., 2017. Optimal quantization scheme for data-efficient target tracking via UWSNs using quantized measurements. *Sensors*, 17(11):2565. https://doi.org/10.3390/s17112565

Zhang ZK, Tian SK, Yang Y, 2023. Node depth adjustment based target tracking in sparse underwater sensor networks. *J Mar Sci Eng*, 11(2):372. https://doi.org/10.3390/jmse11020372

Zhao HY, Yan J, Luo XY, et al., 2021. Ubiquitous tracking for autonomous underwater vehicle with IoUT: a rigid-graph-based solution. *IEEE Int Things J*, 8(18):14094-14109. https://doi.org/10.1109/JIOT.2021.3068090

Zheng LY, Liu MQ, Zhang SL, 2023. An end-to-end sensor scheduling method based on D3QN for underwater passive tracking in UWSNs. *J Netw Comput Appl*, 219:103730. https://doi.org/10.1016/j.jnca.2023.103730